

Language-guided Medical Image Segmentation with Target-informed Multi-level Contrastive Alignments

Mingjian Li¹, Mingyuan Meng¹, Shuchang Ye¹, David Dagan Feng¹, Lei Bi², and Jinman Kim¹

1. *School of Computer Science, The University of Sydney, Australia*

2. *Institute of Translational Medicine, Shanghai Jiao Tong University, China*

Abstract. Medical image segmentation is crucial in modern medical image analysis, which can aid into diagnosis of various disease conditions. Recently, language-guided segmentation methods have shown promising results in automating image segmentation where text reports are incorporated as semantic guidance. These text reports, containing image impressions and insights given by clinicians, provides auxiliary language guidance. However, these methods neglect the inherent pattern gaps between the two distinct modalities, which leads to sub-optimal image-text feature fusion without proper cross-modality feature alignments. Contrastive alignments are widely used to associate image-text semantics in representation learning; however, it has not been exploited to bridge the pattern gaps in language-guided segmentation that relies on subtle low level image details to represent diseases. Existing contrastive alignment methods typically align high-level global image semantics without involving low-level, localized target information, and therefore fails to explore fine-grained text guidance for language-guided segmentation. In this study, we propose a language-guided segmentation network with Target-informed Multi-level Contrastive Alignments (TMCA). TMCA enables target-informed cross-modality alignments and fine-grained text guidance to bridge the pattern gaps in language-guided segmentation. Specifically, we introduce: 1) a target-sensitive semantic distance module that enables granular image-text alignment modelling, and 2) a multi-level alignment strategy that directs text guidance on low-level image features. In addition, a language-guided target enhancement module is proposed to leverage the aligned text to redirect attention to focus on critical localized image features. Extensive experiments on four well-benchmarked image-text datasets, involving three medical imaging modalities, demonstrated that our TMCA achieved superior performances over the state-of-the-art language-guided medical image segmentation methods.

Keywords: Medical image segmentation, Multi-modal Learning, Language-guided segmentation.

1 Introduction

Image segmentation is a fundamental requirement in many medical image analysis tasks. The underlying aim of segmentation is to identify regions of interest (ROIs) in the image, i.e., accurate tumor ROI is a key factor in determining disease's progression and the effectiveness of treatment regimens [1], [2]. Deep learning-based methods have shown promising performance for automatic image segmentation [3]. However, the performance of deep learning-based methods is highly reliant on the availability of manual ROI labels, which are costly to acquire due to the involvement of domain experts. Though self-supervised learning has been exploited to learn without labels, its performance is compromised due to the lack of explicit supervision. Fortunately, medical image text reports, written by clinicians, are readily available alongside the images and contain valuable information including image impressions and insights. Motivated by this, language-guided segmentation methods, that extracts and fuse medical text reports features with image features as auxiliary semantic guidance, have emerged to alleviate the scarcity of labeled medical images and to further refine the segmentation results [4]–[7].

Tomar et al. [7] and Li et al. [4] employed a simple tokenization layer to encode text semantics and then merged them with image features via a attention mechanism. However, such simple tokenization-based text feature extraction methods have difficulties in capturing the high-level text semantics. Lee et al. [6] and Zhong et al. [5] resorted to deep pretrained text encoders to extract high-level semantic text features, which provide a better auxiliary guidance when

fused with image features. However, images and text are inherently encoded in different patterns: images are continuous and rich in details, whereas text is discrete and concise with a focus on high-level concepts. In addition, the encoders used for extracting image and text features are fundamentally different. Despite improved performance, these methods neglected these ‘pattern gaps’ between the extracted image and text features during feature fusion, resulting in sub-optimal information integration and less-effective text guidance for image segmentation.

Recently, vision-language contrastive learning (VLCL) studies attempted to learn general image representations by associating the semantics of paired image-text features through contrastive alignments [8], [9]. Despite its potential to bridge the patten gap, contrastive alignments have not been explored for language-guided segmentation due to the following limitations: Firstly, the segmentation task aims to identify the most informative ROIs (segmentation targets) in the image, making it a localized task rather than one that concerns with the entire image. However, existing contrastive alignment methods typically align entire images and text holistically [8] with assumption that there exists the exact correspondence between the entire image and text, e.g., they are from the same patient. This assumption faces many challenges when aligning images and text pairs from different patients that are not the same but have the similar ROIs. Consequently, these methods may misalign such image and text features, disrupting the feature alignment process and leading to poor feature fusion results. Secondly, segmentation is heavily reliant on subtle image details. Existing contrastive alignment methods typically performed at the deepest level of encoders, which will favor tasks related to the global semantics e.g., image classification. In contrast, image features from the shallow layers of encoders, which are rich in details, receive less direct text guidance.

In this study, we aim to enhance existing language-guided segmentation methods by providing more granular and precise text guidance. Our contributions are as follows:

- a language-guided segmentation network with Target-informed Multi-level Contrastive Alignments (TMCA), which is a new approach that identifies image-text patterns gaps and proposes a contrastive alignments method to bridge the gap;
- a Target-sensitive Semantic Distance Module (TSDM) designed to calculate more granular semantic distance based on the intersection ratios between the ROIs of different images, thereby avoiding misaligning features that describes the same ROIs but differ in less-important backgrounds;
- a multi-level alignment strategy (MAS) to align image and text features at each pyramid feature level, thus enabling a direct guidance on image features derived from shallow layers with rich image details;
- a Language-guided Target Enhancement Module (LTEM) to explicitly associate the text with image sub-regions and then reinforce the identified ROIs though an attention mechanism.

We conducted a thorough evaluation on four well-benchmarked datasets across three different image modalities, including QaTa-COV19 [10] of X-ray images, MosMedData [11] of CT scans, Kvasir-SEG [12] and Bkai-polyp [13] of endoscopic images.. The results show that our TMCA consistently outperforms the state-of-the-art single-modal (image-only) and multi-modal (language-guided) medical image segmentation methods across all metrics, demonstrating the generalizability and effectiveness our method.

2 Related Works

2.1 Deep Learning Based Medical Image Segmentation

The introduction of deep learning-based methods has made substantial advancements in medical image segmentation. The U-Net architecture [14] based on a convolution neural network (CNN) architecture tailored for biomedical image segmentation has demonstrated outstanding performance. The U-shaped architecture in U-Net is composed of a contracting pathway for contextual understanding and a corresponding symmetric expanding pathway for accurate localization of ROIs. This structure is shown to be instrumental in learning detailed feature representations at multiple scales for precise segmentation of ROIs. U-Net++ [15] then re-vamped the skip connection to further mitigate the semantic gaps between encoder and decoder feature maps. Attention U-Net [16] introduced an attention gate to focus on ROIs and to suppress backgrounds. Swin UNETR [17] introduced transformers with shifted window to better capture long-range dependencies across image sub-regions. On the other hand, Isensee et al. [18] proposed nnU-Net to automate the optimal configuration process of U-Net. Ma et al. [19] and Cheng et al. [20] proposed to train general

foundation segmentation model medSAM on large-scale medical image dataset and demonstrated better generalizability than specialized models trained for each individual datasets. Although deep learning has made impressive advancements in the realm of medical image analysis [1], [21], the success of these methods is greatly dependent on the extent availability of annotated training images, which are usually tedious and time-consuming to annotate and difficult to acquire due to various ethics constraints.

To mitigate the restrictions from limited annotations, the use of all accessible data to enhance outcomes is an area of growing importance. For instance, deep learning-based multimodal (image + image) segmentation networks that utilize multimodality medical images are gaining prominence over single-modal methods. Kamnitsas et al. [22] proposed a method that combines multiple CNNs, each trained on different imaging modalities, with their outputs merged by averaging the individual network predictions. Guo et al. [23] investigated three distinct strategies for integrating multi-modal medical imaging data, noting that fusing data within the network provided superior results when compared to combining the outcomes of post-processing, such as with voting based methods. Nevertheless, these approaches often face difficulties in obtaining paired multi-modal medical images due to the limitations of imaging hardware.

2.2 Language-guided Medical Image Segmentation

Recently, auxiliary semantics derived from the text have also been exploited to mitigate the limitations posed by lack of annotations [4]. Medical image text reports, written by clinical experts in their routine workflow, contain image impressions and insights from interpreting the image, and this information can be readily accessed alongside the images.

Tomar et al. [7] extracted text semantics using byte-pair encoding and employed it as a soft channel attention to reinforce the representative features and suppress the less-important features. In this way, the semantic information encoded in the text can be utilized to guide the image segmentation. Li et al. [4] proposed LViT, a dual-U structure consisting of a U-shaped CNN branch alongside a U-shaped Visual Transformer (ViT) [24] branch. This model extracted the fused image and text features within the U-shaped ViT branch and then further integrated them via a Pixel-Level Attention Module (PLAM). The text-enhanced image features were then fed into the CNN decoder. However, LViT initially extracted the text features via a simple vectorization operation, which cannot capture the rich semantics. To mitigate this, Lee et al. [6] employed the text encoder of CLIP [25], which was pretrained on a large language corpus and proven the effectiveness for various textual tasks for feature extraction. After that, they proposed a text-guided cross-position attention module to merge extracted text features with the image features at the bottleneck stage. Hu et al. [26] proposed to extract image features from the pretrained Segment Anything Model (SAM) [27] and simultaneously extract text features from the pretrained BERT [28] model. These features are then combined using multi-layer cross-attention modules and inputted into the segmentation decoder. To accommodate various medical concepts and specialized knowledge in medical text reports, Zhong et al. [5] proposed to employ a medical domain-specific text encoder, CXR-BERT [29], to extract text features encoded with rich semantics and then fuse them with image features at the decoder stage. These methods have outperformed image-only segmentation methods, highlighting the potentials of language-guided medical image segmentation. Nonetheless, these methods primarily focused on the feature extraction and feature fusion strategies, neglecting the inherent huge pattern gaps between the two distinct image-text modalities. This gap may compromise information fusion performance and thus limiting the textual semantic guidance in medical image segmentation.

2.3 Contrastive Alignment

Vision-language contrastive learning is an emerging technique that learns the general image representations from language supervision, where text act as “pseudo instance-level classification labels”. CLIP [25] was the pioneering work that by contrasting the image-text with over 400 million image-text pairs. Zhang et al. [8] introduced contrastive learning to the medical imaging domain. Specifically, it minimized the distance between paired image and text features from the same patient (aligned), while maximizing the distance between non-paired image-text features from different patients (unaligned). Subsequently, Wang et al. [30] extended it with multi-granularity feature alignment, and Wu et al. [31] investigated the explicit encoding of prior medical domain knowledge. The image representations obtained from these studies can be transferred to various downstream tasks such as classification, detection, and segmentation [9]. However, only the pretrained image encoder was utilized in the downstream single-modal segmentation model,

while the text guidance and the decoder part were not involved. The results may be compromised when compared to a multi-modal language-guided segmentation model [4] trained in an end-to-end manner. In this study, we explored a different approach by employing contrastive alignment to bridge cross-modality pattern gaps in a multi-modal model and train them in a simultaneous manner. This allows both text and image features can be better utilized and integrated for language-guided medical image segmentation tasks.

Additionally, medical images and reports from different cases could have large similarity, such as describing similar diseases. Existing contrastive alignment at the patient instance level may inadequately model these similarities. Recently, Wang et al. [32] proposed to calculate alignment distance targets in a more fine-grained manner. For example, smaller alignment distance targets are assigned when different patients have similar classification labels. Similarly, Liu et al. [33] suggested to use text feature similarities for a more semantically aware alignment target. However, these methods are suited for classification tasks rather than segmentation tasks, where the classification labels can be the same, however, the lesion locations and shapes may vary substantially. In contrast, our TSDM is tailored for segmentation task, focusing on localized, target-sensitive alignment for the critical regions e.g., tumor regions.

3 Methods

The architecture of our TMCA is illustrated in Fig. 1. TMCA consists of four components: the image encoder and the text encoder (detailed in Section 3.1), multi-level contrastive alignments with target-sensitive semantic distance module (detailed in Section 3.2), language-guided target enhancement module (detailed in Section 3.3), and language-guided decoder (detailed in Section 3.4).

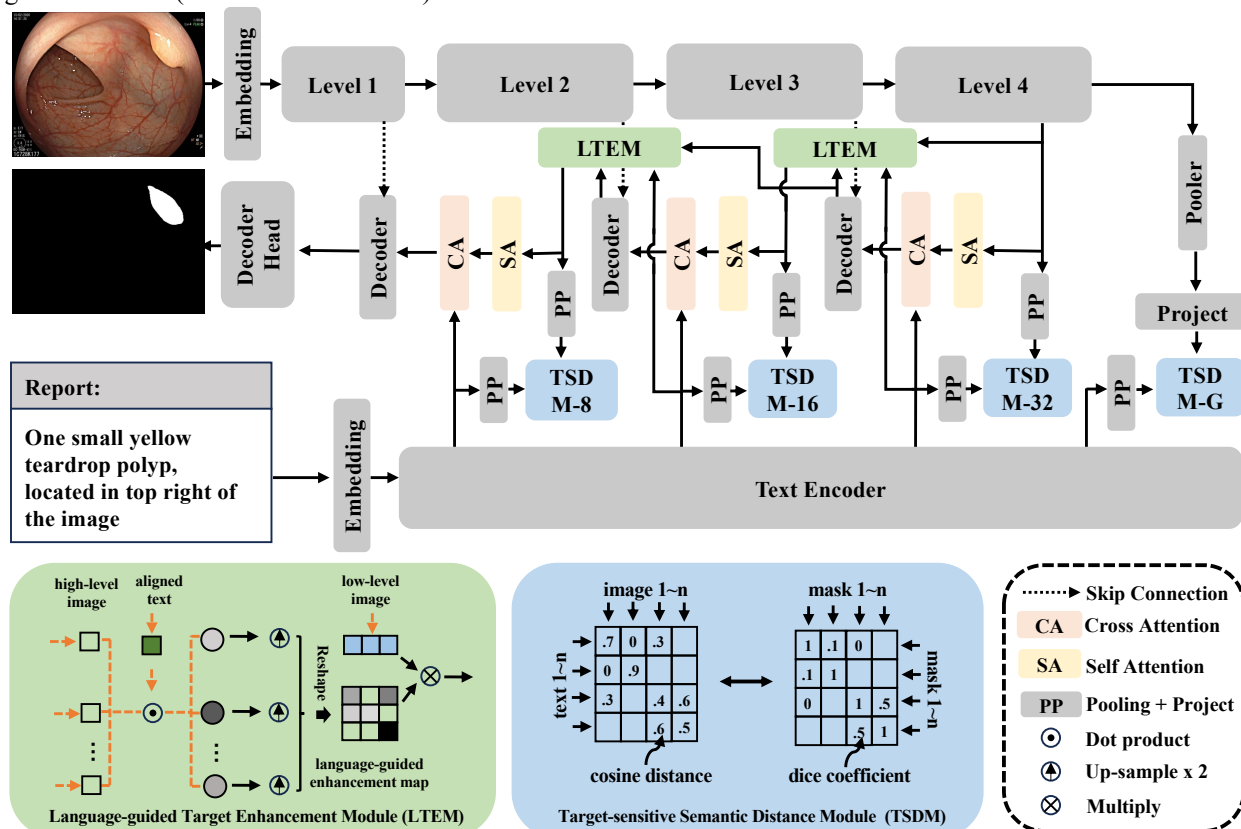


Fig. 1. Overview of our TMCA.

3.1 Image Encoder and Text Encoder

ConvNeXt-Tiny [34] was used as the image encoder following the work in [5]. For each input image, multi-level visual features were extracted from different levels of the image encoder, which is denoted as $I \in \mathbb{R}^C$. The H and W are the height and width of the input image and C is the feature dimension, respectively. The global image feature was also extracted after the pooling layer of the image encoder, which is denoted as I_g .

The medical domain-specific language model CXR-BERT [29] was employed as the text encoder. The CXR-BERT was pretrained on medical imaging reports and has demonstrated superior capability in extraction textual semantics. Specifically, K word features were extracted from the last 3 layers of the CXR-BERT, and the text feature T for each word is defined as the averages across these 3 layers.

3.2 Target-sensitive semantic distance module

The aim of our segmentation-tailored contrastive alignment with the target-sensitive semantic distance module (TSDM) is to bridge the pattern gaps between the two distinct modalities of image and text. Standard contrastive alignment attempts to maximize the similarity between paired image-text samples from the same patient, while minimizing the similarity between non-paired samples. The underlying assumption is that the semantics of the image and text from the same patient are identical. Maximizing the similarities between images and texts would allow to align their features. However, similarities between medical images and text exhibit multi-granularity properties [30], for example the semantics of images and text from different patients but describing similar diseases can be highly similar as well.

For segmentation task, the segmentation mask clearly delineates the target-related image regions that contain critical semantics. We thus employed the intersections of different image masks to model the semantic distance between different patients in a target-sensitive manner. Specifically, in contrastive alignment target construction, the distance $d_{p,q}$ for any sampled image (from the p -th pair) and text (from q -th pair) is defined by the Dice coefficient between their corresponding segmentation masks. A SoftMax was then applied to normalize $d_{p,q}$ across the batch dimension with the temperature τ_1 .

The model then predicted the current similarity distance between the image and the text. We firstly projected text features into the dimension of image features at each level through a projection head. The cosine distance $s_{p,q}$ between the p -th image feature and the q -th text feature was then calculated and normalized with the SoftMax layer with a temperature τ_2 . We employed the tailored semantic contrastive loss as the objective function, calculated as a cross-entropy loss between the predicted similarity $s_{p,q}$ and the target-sensitive semantic distance $d_{p,q}$:

$$L = -\frac{1}{BZ} \sum \sum d_{p,q} * \log(s_{p,q}) \quad (1)$$

where BZ is the batch size. In our implementation, we computed the cross-entropy loss in both image-to-text and text-to-image directions and then averaged them to derive the bi-directional contrastive loss.

In addition, we applied a multi-level alignment strategy (MAS) to bridge pattern gaps between image-text features at multiple levels. Specifically, the contrastive alignments were added at image levels with strides equal to 8, 16, 32 and these were denoted as TSDM-8/16/32, respectively. The contrastive alignment module at the deepest level was demoted as TSDM-G. The final multi-level contrastive alignments loss L_{CA} was defined as the average of bi-directional contrastive losses across all the levels.

3.3 Language-guided target enhancement module

The aim of our language-guided target enhancement module is to exploit the aligned text to guide the model in selectively enhancing critical image regions. Since the deep layers of convolutional neural networks tend to contain high-level semantic information, while the shallow layers tend to contain more low-level and detailed class-agnostic information [35], we employed the language-guided cross-attention map on deep layers to guide the low-level decoded features. Initially, we calculated the normalized dot product similarity between the i -th high-level image sub-region features I_i and the global text feature, which can be defined as:

$$w_i = I_i^T T_g \quad (2)$$

Then we normalized w_i across the image sub-region dimension using the SoftMax with the temperature τ_3 . The normalized target-informed attention map was reshaped and upsampled by a factor of 2. Finally, it was multiplied by

the decoded image features, which has been combined with the shallow layer skip-connected image features. This language-guided target enhanced decoded image feature was then passed into the next language-guided decoder.

3.4 Language-guided decoder

The language-guided decoder progressively combines the aligned image and text information for segmentation prediction. Initially, the aligned image feature was added with a positional embedding and a self-attention (SA) module to capture the long-range intro-modality relations and to aggregate global semantics. The enhanced image features are denoted as I' . Subsequently, a multi-head cross-attention (CA) module with a skip-connection was adopted to fuse the aligned image and text features T' . In this process, the image features served as the Q and text features served as the K and V , which are defined as:

$$f_s = CA(I', T') \quad (3)$$

The term f_s refers to the feature that integrate information from both images and text. The semantics encoded in the text features could serve as an auxiliary guidance for the decoder side. After that, a standard U-shape image decoder was applied. A deconvolution layer was applied to upsample f_s by a factor of 2, and a skip connection from the encoder feature map was also attached to retain the low-level localized features. The segmentation loss L_{SEG} was defined as the sum of Dice Loss and Cross-Entropy Loss. The final loss of the whole network is formulated as the summation of the multi-level contrastive alignment loss and the segmentation loss, which is:

$$L = L_{CA} + L_{SEG} \quad (4)$$

At the inference, the text prompt and the extracted text features were firstly fused with the image features, which was then used to guide the image segmentation.

4 Experimental Setup

4.1 Datasets

TMCA was evaluated with the following datasets: QaTa-COV19 [10], MosMedData [11], Kvasir-SEG [12] and Bkai-polyp [13]. The QaTa-COV19 dataset contains 9258 COVID-19 Chest X-rays and ground-truth segmentation annotations for the COVID-19 infected regions. The MosMedData dataset contains 2729 CT scan slices of opacifications and consolidations. Li et al. [4] extended these two datasets with matched text reports. Each text report consists of three sentences: the first sentence indicates the presence of infection, the second sentence outlines the count of infected regions, and the third sentence describes the location of these infected regions. This text report provides rich semantics that can be used to guide the lesion segmentation.

Both the Kvasir-SEG and Bkai-polyp datasets contain 1000 endoscopic images with ground-truth segmentation labels of gastrointestinal polyps. Poudel et al. [36] extended these two datasets with matched text reports, containing information on size, count, color, and location in a free text format, such as “two large white round polyp, located in top left, top of the image”.

The official training set of the QaTa-COV19 dataset contains 7145 samples, while the test set contains over 2113 samples. Following the work proposed in Ariadne [5], the official training set was split into train and validation sets with a distribution of 80% and 20%. For the MosMedData dataset, we followed the train/validation/test split in LViT [4]. Similarly, we followed the work in [36] to split the train/validation/test for the Kvasir-SEG and Bkai-polyp datasets.

4.2 Implementation Details

All images were resized to a dimension of 224×224 . Image augmentation was applied by random zoom in with a 10% probability [5]. PyTorch framework was employed with the PyTorch Lightning as the wrapper for training and testing. The proposed method was trained using a Nvidia 24 GB RTX3090 GPU with a batch size of 32. AdamW optimizer was used with a learning rate set to $3e^{-4}$. Additionally, a cosine annealing scheduler was employed with the minimal learning rate set to $1e^{-6}$. Our code will be publicly available on GitHub upon publication.

4.3 Experimental Settings

TMCA was firstly benchmarked against state-of-the-art single-modal (image-only) segmentation methods and multi-modal (language-guided) segmentation methods. All single-modal methods were extensions of U-Net [14] which has become the default baseline for medical image segmentation due to its strong performance. U-Net++ [15] re-vamped the skip connection to mitigate the semantic gaps between encoder and decoder feature maps. Attention U-Net [16] introduced an attention gate to focus on ROIs and suppressed backgrounds. nnU-Net [18] automated the optimization of U-Net configuration.

For multi-modal (image and text) methods, TGANet [7] introduced the text guidance for image segmentation. LViT [4] employed a U-shape ViT to integrate text and image semantics. LGA [26] inserted multiple feature fusion modules as the language guided adapter for the image encoder. CPAM [6] proposed cross-position attention for joint text-image information processing. Ariadne [5] progressively incorporated text information into image decoders, and thus improving the overall segmentation performance.

Additionally, three ablation studies were carried out: 1) we investigated the effect of each component of the proposed TMCA by progressively ablating each component, 2) we measured the effect of different settings of our MAS, and 3) we investigated the efficiency in data utilization of the proposed TMCA.

Following LViT [4], two commonly used segmentation evaluation metrics were employed: Jaccard coefficient (Jaccard) and Dice similarity coefficient (Dice). Both of these coefficients access the ratio of the intersection over a function of the size of the individual sets or their union. In general, a higher Jaccard coefficient or a higher Dice coefficient indicates a better segmentation result. Notably, the Dice is more sensitive to small targets [5].

5 Results

5.1 Comparison to the State-of-the-Art

Table 1 shows the segmentation results. Single-modal and Multi-modal refer to models without or with text guidance, respectively. Overall, our TMCA consistently outperformed the comparison methods. For the QaTa-COV19 dataset, U-Net++ achieved the best performance among the single-modal methods, while Ariadne achieved the second best performance among multi-modal methods. Our TMCA outperformed the U-Net++ by 11.31% in Jaccard and 7.18% in Dice, and also outperformed Ariadne by 1.82% in Jaccard on QaTA-COV19. For the MosMedData dataset, nnU-Net and Ariadne achieved the best performance for the single-modal methods and the multi-modal methods, respectively. Our TMCA further improved the nnU-Net by 3.91% in Jaccard and 5.66% in Dice, and also improved the Ariadne by 1.23% in Jaccard. For polyp segmentation, our TMCA outperformed the state-of-the-art by 2.24% and 1.89% in Jaccard for the Kvasir-SEG and Bkai-polyp datasets, respectively.

Table 1. Results of segmentation of the TMCA method and the comparison methods. The best and the second-best results are highlighted in bold and underlined, respectively.

Methods	QaTa-COV19		MosMedData		Kvasir-SEG		Bkai-polyp	
	Jaccard (%)	Dice (%)	Jaccard (%)	Dice (%)	Jaccard (%)	Dice (%)	Jaccard (%)	Dice (%)
<i>Single-Modal</i>								
U-Net [14]	70.92	82.99	50.73	64.60	69.62	82.09	79.06	88.31
U-Net++ [15]	71.96	83.69	58.39	71.75	69.58	82.06	79.87	88.81
nnU-Net [18]	70.81	80.42	60.36	72.59	-	-	-	-
Attention U-Net [16]	70.06	82.40	52.82	66.34	74.19	85.18	72.97	84.26
<i>Multi-Modal</i>								
LViT [4]	73.79	84.92	61.33	74.57	77.04	87.03	75.19	85.84
CPAM [6]	75.98	84.25	-	-	-	-	-	-
TGANet [7]	70.75	79.87	59.28	71.81	<u>83.30</u>	<u>89.82</u>	84.09	90.23
Ariadne [5]	<u>81.45</u>	<u>89.78</u>	<u>63.04</u>	<u>77.33</u>	80.70	89.32	<u>88.02</u>	<u>93.63</u>
LGA [26]	76.23	84.65	62.52	75.63	-	-	-	-
TMCA (Ours)	83.27	90.87	64.27	78.25	85.54	92.20	89.91	94.69

5.2 Ablation Study

Table 2 presents the ablation study results of our TMCA exemplified on the Kvasir-SEG dataset. The performances gradually decreased as each component was incrementally removed from TMCA. All the components contributed to the final performance with the contrastive alignment component resulted in the highest performance improvement with an increase of 1.69% in Jaccard.

Table 2. Ablation results of each component of our TMCA.

Ablation Components	Kvasir-SEG		
	Jaccard (%)	Accuracy (%)	Dice (%)
TMCA (Ours)	85.54	97.82	92.20
-TSDM	84.58	97.65	91.64
-LTEM	83.41	97.46	90.96
-MAS	82.39	97.30	90.34
-Contrastive Alignment	80.70	97.12	89.32

Table 3 shows the results when applied the proposed contrastive alignment components at different encoder levels with various strides. The results indicate a consistent enhancement of segmentation performance with the inclusion of our contrastive alignment (w/ TSDM and LTEM). Employing multi-level contrastive alignment, which involved progressively adding contrastive alignment starting from only TSDM-G, further improved the results. The final model which applied contrastive alignment across all levels attained the best results with an increase of 4.84% in Jaccard.

Table 3. Ablation study results of our multi-level contrastive alignments strategy.

Methods	Kvasir-SEG		
	Jaccard (%)	Accuracy (%)	Dice (%)
baseline	80.70	97.12	89.32
+ TSDM-G	82.30	97.29	90.23
+ TSDM-G/32	83.74	97.55	91.14
+ TSDM-G/32/16	84.35	97.63	91.51
+ TSDM-G/32/16/8	85.54	97.82	92.20

Table 4 shows the results using different ratios of data for training. Our TMCA trained with only 25% data outperformed single-modal method Attention U-Net with 100% data, by 4.05% on Jaccard, and 2.61% on Dice score. The TMCA with 75% data outperformed all other comparison methods with 100% data, including multi-modal methods such as TGANet.

Table 4. Ablation study results of our multi-level contrastive alignments strategy.

Methods	Data Ratio	Kvasir-SEG		
		Jaccard (%)	Accuracy (%)	Dice (%)
Attention U-Net [16]	100%	74.19	-	85.18
TGANet [7]	100%	83.30	-	89.82
TMCA	25%	78.24	96.48	87.79
TMCA	50%	81.67	97.21	89.91
TMCA	75%	84.78	97.72	91.76
TMCA	100%	85.54	97.82	92.20

5.3 Qualitative Results and Analysis

Fig. 2. shows the qualitative results of our TMCA and comparison methods across four datasets. The results demonstrate that our TMCA can accurately segment lesions with the text guidance, even in scenarios of low image contrast and image quality (row 1, 2, 3 and 5). In contrast, other methods, especially single-modal methods, tend to produce false positive segmentation results (row1-7) and/or fail to segment lesion regions with low contrast to the background (row 2,5, and 6). Multi-modal methods like LViT and Ariadne utilized text guidance to reduce false positive regions (e.g., row 1, where the text specifies there are no infected area in left lung region) and for segmenting the challenging regions (e.g., row 6, where the text indicates that there is a polyp at the top of the image). Additionally, our TMCA refines the guidance through the proposed TSDM and apply it to subtle image details through the proposed MAS and LTEM, achieving the most accurate segmentation results.



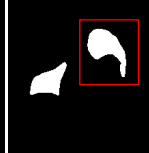

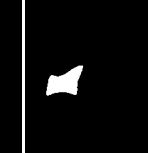
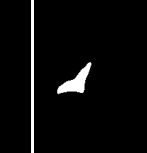
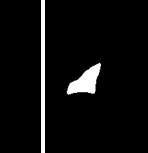


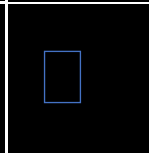
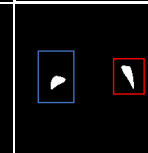
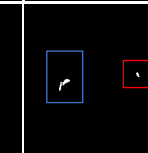
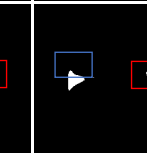
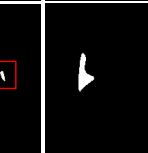
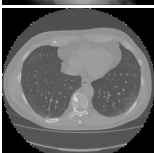
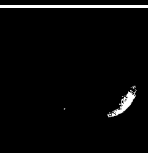
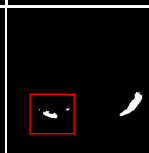
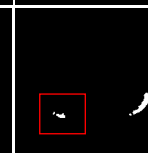




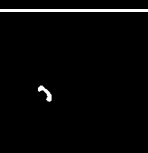
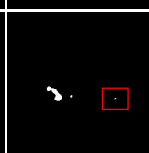
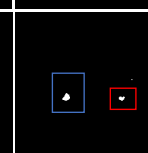
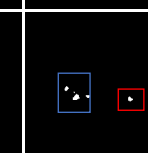
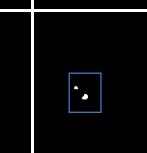
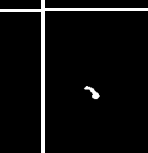

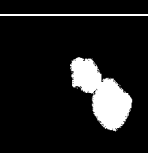
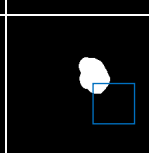
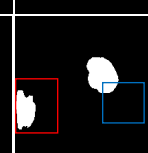
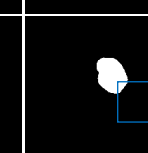
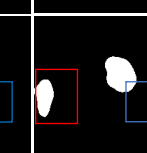
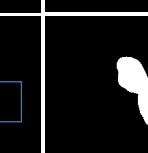
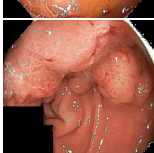

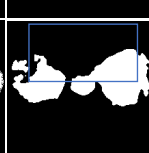
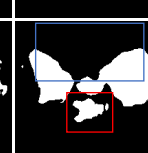



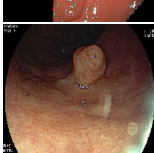
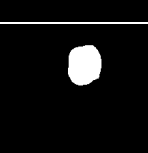

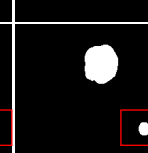
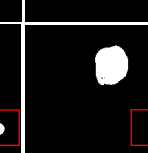
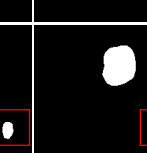
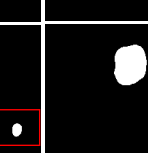
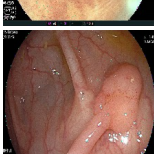

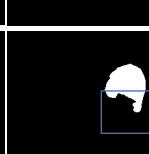
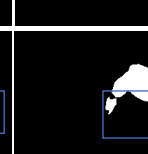
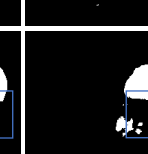


	Unilateral pulmonary infection, one infected area, right lung						
	Unilateral pulmonary infection, one infected area, middle right lung						
	Unilateral pulmonary infection, one infected areas, middle left lung						
	Unilateral pulmonary infection, one infected area, middle right lung						
	one medium white heart polyp, located in right of the image						
	Two large white round polyp, located in top left, top of the image						
	one small brown oval polyp, located in top right of the image						
	One medium white circle polyp, located in right of the image						
Image	Text Prompt	Ground Truth	U-Net (Single-Modal)	U-Net++ (Single-Modal)	LViT (Multi-Modal)	Ariadne (Multi-Modal)	TMCA (Multi-Modal)

Fig. 2. Qualitative results on the four datasets, from row 1 to row 8: (1-2) QaTa-COV19, (3-4) MosMedData, (5-6) Kvasir-SEG and, (7-8) Bkai-polyp. Red boxes indicate the regions falsely identified (false positive) and blue boxes indicate the regions not identified (false negative). Our TMCA method produced the best results compared to other methods.

6 Discussion

Our main findings are as follows: (1) our TMCA outperformed the state-of-the-art segmentation methods, including both single-modal (image-only) and multi-modal (language-guided) segmentation methods; (2) the proposed TMCA with only 10% training data outperformed the existing single-modal methods; (3) the proposed TSDM and LTEM enhanced the segmentation performance by enabling more fine-grained text guidance on critical image regions; and (4) the proposed multi-level contrastive alignment strategy surpassed the existing single-level contrastive alignment strategy.

The TMCA outperformed the state-of-the-art methods on all metrics (Table 1). The multi-modal methods employing text guidance including LViT, CPAM, Ariadne and TMCA consistently outperformed single-modal segmentation methods such as U-Net. This is attributed to the integration of additional textual information. The results of LViT were less favourable among all language-guided methods. This is likely attributed to the fact that LViT employed a simple tokenization layer to encode text features before integrating with image features, which limits its ability to capture the high-level text semantics. Ariadne ranked the second-best overall and this can be attributed to the employment of a well-pretrained deep text encoder that is capable of extracting rich, high-level text semantics. TMCA consistently outperformed the Ariadne and we attribute this improvement to the TMCA providing additional alignment between the text features and the image features, which reduces the pattern gaps between the image and text during feature integration. This is evidenced in the last row of Table 2. The performance improvements are observed by merely incorporating contrastive alignment (in the second last row) compared to the last row (Ariadne). Figure 2 shows that for the hard negative cases, TMCA could more precisely employ the semantics in text prompts to guide the segmentation.

TMCA outperformed all single-modal image segmentation methods with the use of only 25% of training data (Table 4). This is attributed to the integration of additional textual information, which showcases the potential to mitigate the scarcity of image annotations for deep learning-based segmentation methods. Furthermore, TMCA trained with only 75% of the training data (Table 4) outperformed all the comparison multi-modal methods using 100% of the training data (Table 1), highlighting the capabilities in data efficiencies.

The proposed TSDM and LTEM both improved the segmentation performance (Table 2). This is attributed to the fact that our TSDM and LTEM can enable the model to focus on small critical image regions which characterize the medical images. Existing contrastive alignment methods aligned the entire image and text holistically, such that cannot align images and text pairs that have high similarities in disease-related regions but low similarities in other regions. This inevitably introduces false negatives during the contrastive alignment. Moreover, for medical image analysis tasks, important information tends to only occupy a small portion of the medical image and its associated text (disease, location, severity etc.). These subtle yet critical information may be overlooked by the extensive non-critical information such as the description of healthy regions. Our TSDM calculates the similarity or contrastive distance based on the interaction of the segmentation masks, which eliminates the redundant information and allows to focus on the most critical disease-related information in contrastive alignment. Additionally, with image-text features aligned, our LTEM identifies the most critical image regions through cross-attention from the text on the image and then reinforces these regions, which is an essential step for accurate segmentation. This observation also aligned with the widely employed spatial attention mechanism [37].

TMCA yielded larger improvements when multi-level contrastive alignments were involved (Table 3, starting from TSDM-G and progressively adding TSDM at each shallower level). This is attributed to fact that more fine-grained text guidance is integrated on each level of the image decoder. When only deepest layer’s text and image features were aligned through contrastive alignment, the information integration at the shallow layers might become confused and the decoded image feature might be directed to less-important regions. These shallow layers, which focus on local image details such as the boundaries of the regions of interest (ROIs), are heavily reliant on high level image semantic features and auxiliary text features to offer high level guidance on attentive regions. By incorporating multi-level intermediate contrastive alignments, TMCA effectively aligns text features at each level, facilitating better integration with image features. It also enables our LTEM, which associates each image sub-regions with text by calculating their feature similarities, to provide more accurate localization guidance. This is particularly important for medical image

segmentation where targets are typically small and rely on the shallow layers of the model. This observation is also consistent with deep supervision works, where intermediate supervision or auxiliary supervision provides additional supervision at hidden layers of a neural network [38], [39].

The language-guided image segmentation has been proven to be useful in practical scenarios where clinicians can provide text based interactive guidance [4]. However, the text prompts used in the existing studies are usually crafted to be concise for denoting the ROIs, for example, “one small brown oval polyp, located in top right of the image”. This may not fully reflect routine clinical workflow, in which the text reports are more complex and descriptive with referral to the patient’s historical medical records. This may be mitigated through more advanced NLP preprocessing techniques, for example, lengthy text reports can be refined and structured using large language models (LLMs) [40], [41] as the preprocess. The proposed language-guided image segmentation can then be subsequently applied to the preprocessed text inputs. In addition, in future work, we also plan to curate the segmentation datasets in together with real complex text reports to further evaluate the generalizability of the proposed method.

7 Conclusion

We have outlined a language-guided segmentation network (TMCA) with multi-level fine-grained target-sensitive contrastive alignments for medical images. Unlike existing methods that overlook the inherent image-text pattern gaps, our image-text contrastive alignment (CA) module explicitly bridges this gap to optimize information integration. We particularly identified that our TSDM and LTEM were able to leverage more fine-grained text guidance on small and critical image regions. In addition, our MAS promoted more direct and efficient text guidance across all image feature resolutions. The experimental results show that our TMCA consistently outperforms state-of-the-art segmentation methods on four well-benchmarked datasets for medical image segmentation, which demonstrates strong generalizability.

References

- [1] X. Chen, X. Wang, K. Zhang, K.-M. Fung, T. C. Thai, K. Moore, R. S. Mannel, H. Liu, B. Zheng, and Y. Qiu, “Recent advances and clinical applications of deep learning in medical image analysis,” *Medical Image Analysis*, p. 102444, 2022.
- [2] X. Jiang, Z. Hu, S. Wang, and Y. Zhang, “Deep Learning for Medical Image-Based Cancer Diagnosis,” *Cancers*, vol. 15, no. 14, p. 3608, Jan. 2023.
- [3] R. Wang, T. Lei, R. Cui, B. Zhang, H. Meng, and A. K. Nandi, “Medical image segmentation using deep learning: A survey,” *IET Image Processing*, vol. 16, no. 5, pp. 1243–1267, 2022.
- [4] Z. Li, Y. Li, Q. Li, P. Wang, D. Guo, L. Lu, D. Jin, Y. Zhang, and Q. Hong, “LViT: Language meets Vision Transformer in Medical Image Segmentation,” *IEEE Transactions on Medical Imaging*, pp. 1–1, 2023.
- [5] Y. Zhong, M. Xu, K. Liang, K. Chen, and M. Wu, “Ariadne’s Thread: Using Text Prompts to Improve Segmentation of Infected Areas from Chest X-ray Images,” in *Medical Image Computing and Computer Assisted Intervention – MICCAI 2023*, Cham, 2023, pp. 724–733.
- [6] G.-E. Lee, S. H. Kim, J. Cho, S. T. Choi, and S.-I. Choi, “Text-Guided Cross-Position Attention for Segmentation: Case of Medical Image,” in *Medical Image Computing and Computer Assisted Intervention – MICCAI 2023*, Cham, 2023, pp. 537–546.
- [7] N. K. Tomar, D. Jha, U. Bagci, and S. Ali, “TGANet: Text-Guided Attention for Improved Polyp Segmentation,” in *Medical Image Computing and Computer Assisted Intervention – MICCAI 2022*, Cham, 2022, pp. 151–160.
- [8] Y. Zhang, H. Jiang, Y. Miura, C. D. Manning, and C. P. Langlotz, “Contrastive learning of medical visual representations from paired images and text,” in *Machine Learning for Healthcare Conference, 2022*, pp. 2–25.
- [9] Z. Zhao, Y. Liu, H. Wu, Y. Li, S. Wang, L. Teng, D. Liu, Z. Cui, Q. Wang, and D. Shen, “CLIP in Medical Imaging: A Comprehensive Survey.” arXiv, 14-Dec-2023.
- [10] A. Degerli, S. Kiranyaz, M. E. Chowdhury, and M. Gabbouj, “Osegnet: Operational segmentation network for COVID-19 detection using chest X-ray images,” in *2022 IEEE International Conference on Image Processing (ICIP)*, 2022, pp. 2306–2310.
- [11] S. P. Morozov, A. E. Andreychenko, N. A. Pavlov, A. V. Vladzimirskyy, N. V. Ledikhova, V. A. Gombolevskiy, I. A. Blokhin, P. B. Gelezhe, A. V. Gonchar, and V. Y. Chernina, “MosMedData: Chest CT Scans With COVID-19 Related Findings Dataset.” arXiv, 13-May-2020.

- [12] D. Jha, P. H. Smedsrud, M. A. Riegler, P. Halvorsen, T. De Lange, D. Johansen, and H. D. Johansen, “Kvasir-SEG: A Segmented Polyp Dataset,” in *MultiMedia Modeling*, vol. 11962, Y. M. Ro, W.-H. Cheng, J. Kim, W.-T. Chu, P. Cui, J.-W. Choi, M.-C. Hu, and W. De Neve, Eds. Cham: Springer International Publishing, 2020, pp. 451–462.
- [13] P. Ngoc Lan, N. S. An, D. V. Hang, D. V. Long, T. Q. Trung, N. T. Thuy, and D. V. Sang, “NeoUNet : Towards Accurate Colon Polyp Segmentation and Neoplasm Detection,” in *Advances in Visual Computing*, Cham, 2021, pp. 15–28.
- [14] O. Ronneberger, P. Fischer, and T. Brox, “U-net: Convolutional networks for biomedical image segmentation,” in *International Conference on Medical image computing and computer-assisted intervention*, 2015, pp. 234–241.
- [15] Z. Zhou, M. M. Rahman Siddiquee, N. Tajbakhsh, and J. Liang, “UNet++: A Nested U-Net Architecture for Medical Image Segmentation,” in *Deep Learning in Medical Image Analysis and Multimodal Learning for Clinical Decision Support*, Cham, 2018, pp. 3–11.
- [16] O. Oktay, J. Schlemper, L. L. Folgoc, M. Lee, M. Heinrich, K. Misawa, K. Mori, S. McDonagh, N. Y. Hammerla, and B. Kainz, “Attention u-net: Learning where to look for the pancreas,” *arXiv preprint arXiv:1804.03999*, 2018.
- [17] A. Hatamizadeh, V. Nath, Y. Tang, D. Yang, H. R. Roth, and D. Xu, “Swin UNETR: Swin Transformers for Semantic Segmentation of Brain Tumors in MRI Images,” in *Brainlesion: Glioma, Multiple Sclerosis, Stroke and Traumatic Brain Injuries*, vol. 12962, A. Crimi and S. Bakas, Eds. Cham: Springer International Publishing, 2022, pp. 272–284.
- [18] F. Isensee, P. F. Jaeger, S. A. Kohl, J. Petersen, and K. H. Maier-Hein, “nnU-Net: a self-configuring method for deep learning-based biomedical image segmentation,” *Nature methods*, vol. 18, no. 2, pp. 203–211, 2021.
- [19] J. Ma, Y. He, F. Li, L. Han, C. You, and B. Wang, “Segment anything in medical images,” *Nat Commun*, vol. 15, no. 1, p. 654, Jan. 2024.
- [20] J. Cheng, J. Ye, Z. Deng, J. Chen, T. Li, H. Wang, Y. Su, Z. Huang, J. Chen, L. Jiang, H. Sun, J. He, S. Zhang, M. Zhu, and Y. Qiao, “SAM-Med2D.” *arXiv*, 30-Aug-2023.
- [21] D. Shen, G. Wu, and H.-I. Suk, “Deep learning in medical image analysis,” *Annual review of biomedical engineering*, vol. 19, pp. 221–248, 2017.
- [22] K. Kamnitsas, W. Bai, E. Ferrante, S. McDonagh, M. Sinclair, N. Pawlowski, M. Rajchl, M. Lee, B. Kainz, D. Rueckert, and B. Glocker, “Ensembles of Multiple Models and Architectures for Robust Brain Tumour Segmentation,” in *Brainlesion: Glioma, Multiple Sclerosis, Stroke and Traumatic Brain Injuries*, Cham, 2018, pp. 450–462.
- [23] Z. Guo, X. Li, H. Huang, N. Guo, and Q. Li, “Deep Learning-Based Image Segmentation on Multimodal Medical Imaging,” *IEEE Transactions on Radiation and Plasma Medical Sciences*, vol. 3, no. 2, pp. 162–169, Mar. 2019.
- [24] A. Dosovitskiy, L. Beyer, A. Kolesnikov, D. Weissenborn, X. Zhai, T. Unterthiner, M. Dehghani, M. Minderer, G. Heigold, and S. Gelly, “An image is worth 16x16 words: Transformers for image recognition at scale,” *arXiv preprint arXiv:2010.11929*, 2020.
- [25] A. Radford, J. W. Kim, C. Hallacy, A. Ramesh, G. Goh, S. Agarwal, G. Sastry, A. Askell, P. Mishkin, J. Clark, G. Krueger, and I. Sutskever, “Learning Transferable Visual Models From Natural Language Supervision,” *arXiv:2103.00020 [cs]*, Feb. 2021.
- [26] J. Hu, Y. Li, H. Sun, Y. Song, C. Zhang, L. Lin, and Y.-W. Chen, “LGA: A Language Guide Adapter for Advancing the SAM Model’s Capabilities in Medical Image Segmentation,” in *Medical Image Computing and Computer Assisted Intervention – MICCAI 2024*, Cham, 2024, pp. 610–620.
- [27] A. Kirillov, E. Mintun, N. Ravi, H. Mao, C. Rolland, L. Gustafson, T. Xiao, S. Whitehead, A. C. Berg, W.-Y. Lo, P. Dollar, and R. Girshick, “Segment Anything,” presented at the Proceedings of the IEEE/CVF International Conference on Computer Vision, 2023, pp. 4015–4026.
- [28] J. Devlin, M.-W. Chang, K. Lee, and K. Toutanova, “BERT: Pre-training of Deep Bidirectional Transformers for Language Understanding.” *arXiv*, 24-May-2019.
- [29] B. Boecking, N. Usuyama, S. Bannur, D. C. Castro, A. Schwaighofer, S. Hyland, M. Wetscherek, T. Naumann, A. Nori, and J. Alvarez-Valle, “Making the Most of Text Semantics to Improve Biomedical Vision–Language Processing,” *arXiv preprint arXiv:2204.09817*, 2022.
- [30] F. Wang, Y. Zhou, S. WANG, V. Vardhanabhuti, and L. Yu, “Multi-granularity cross-modal alignment for generalized medical visual representation learning,” in *Advances in neural information processing systems*, 2022, vol. 35, pp. 33536–33549.
- [31] C. Wu, X. Zhang, Y. Zhang, Y. Wang, and W. Xie, “MedKLLIP: Medical Knowledge Enhanced Language-Image Pre-Training for X-ray Diagnosis,” in *Proceedings of the IEEE/CVF International Conference on Computer Vision (ICCV)*, 2023, pp. 21372–21383.
- [32] Z. Wang, Z. Wu, D. Agarwal, and J. Sun, “MedCLIP: Contrastive Learning from Unpaired Medical Images and Text,” in *Proceedings of the 2022 Conference on Empirical Methods in Natural Language Processing*, Abu Dhabi, United Arab Emirates, 2022, pp. 3876–3887.

- [33] B. Liu, D. Lu, D. Wei, X. Wu, Y. Wang, Y. Zhang, and Y. Zheng, "Improving Medical Vision-Language Contrastive Pretraining with Semantics-aware Triage," *IEEE Transactions on Medical Imaging*, pp. 1–1, 2023.
- [34] Z. Liu, H. Mao, C.-Y. Wu, C. Feichtenhofer, T. Darrell, and S. Xie, "A ConvNet for the 2020s," presented at the Proceedings of the IEEE/CVF Conference on Computer Vision and Pattern Recognition, 2022, pp. 11976–11986.
- [35] R. R. Selvaraju, M. Cogswell, A. Das, R. Vedantam, D. Parikh, and D. Batra, "Grad-CAM: Visual Explanations from Deep Networks via Gradient-based Localization," *Int J Comput Vis*, vol. 128, no. 2, pp. 336–359, Feb. 2020.
- [36] K. Poudel, M. Dhakal, P. Bhandari, R. Adhikari, S. Thapaliya, and B. Khanal, "Exploring Transfer Learning in Medical Image Segmentation using Vision-Language Models." arXiv, 20-Jun-2024.
- [37] J. Hu, L. Shen, and G. Sun, "Squeeze-and-excitation networks," in *Proceedings of the IEEE conference on computer vision and pattern recognition*, 2018, pp. 7132–7141.
- [38] J. Le'Clerc Arrastia, N. Heilenkötter, D. Otero Bager, L. Hauberg-Lotte, T. Boskamp, S. Hetzer, N. Duschner, J. Schaller, and P. Maass, "Deeply Supervised UNet for Semantic Segmentation to Assist Dermatopathological Assessment of Basal Cell Carcinoma," *Journal of Imaging*, vol. 7, no. 4, p. 71, Apr. 2021.
- [39] Z. Zhao, Z. Zeng, K. Xu, C. Chen, and C. Guan, "DSAL: Deeply Supervised Active Learning From Strong and Weak Labelers for Biomedical Image Segmentation," *IEEE Journal of Biomedical and Health Informatics*, vol. 25, no. 10, pp. 3744–3751, Oct. 2021.
- [40] H. Touvron, T. Lavril, G. Izacard, X. Martinet, M.-A. Lachaux, T. Lacroix, B. Rozière, N. Goyal, E. Hambro, F. Azhar, A. Rodriguez, A. Joulin, E. Grave, and G. Lample, "LLaMA: Open and Efficient Foundation Language Models." arXiv, 27-Feb-2023.
- [41] C. Wu, W. Lin, X. Zhang, Y. Zhang, W. Xie, and Y. Wang, "PMC-LLaMA: toward building open-source language models for medicine," *Journal of the American Medical Informatics Association*, p. ocae045, Apr. 2024.